

Large-Scale Gaussian Processes via Alternating Projection

Kaiwen Wu¹ Jonathan Wenger² Haydn Jones¹ Geoff Pleiss^{3,4} Jacob R. Gardner¹

¹University of Pennsylvania ²Columbia University ³University of British Columbia ⁴Vector Institute

Abstract

Gaussian process (GP) hyperparameter optimization requires repeatedly solving linear systems with $n \times n$ kernel matrices. To address the prohibitive $\mathcal{O}(n^3)$ time complexity, recent work has employed fast iterative numerical methods, like conjugate gradients (CG). However, as datasets increase in magnitude, the corresponding kernel matrices become increasingly ill-conditioned and still require $\mathcal{O}(n^2)$ space without partitioning. Thus, while CG increases the size of datasets GPs can be trained on, modern datasets reach scales beyond its applicability. In this work, we propose an iterative method which only accesses subblocks of the kernel matrix, effectively enabling *mini-batching*. Our algorithm, based on alternating projection, has $\mathcal{O}(n)$ per-iteration time and space complexity, solving many of the practical challenges of scaling GPs to very large datasets. Theoretically, we prove our method enjoys linear convergence and empirically we demonstrate its robustness to ill-conditioning. On large-scale benchmark datasets up to four million datapoints our approach accelerates training by a factor of $2\times$ to $27\times$ compared to CG.

1 INTRODUCTION

Scaling Gaussian process (GP) models to large datasets has been a central research topic in probabilistic machine learning for nearly two decades. The primary challenge is the cubic complexity of computing both the marginal log likelihood (MLL) during training and the predictive distribution at test time. Over the years, this problem has been addressed both

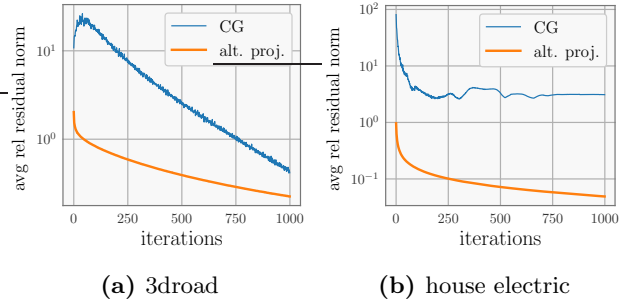


Figure 1: Comparison of the convergence of alternating projection and (preconditioned) conjugate gradient. Both algorithms are *initialized at zero*, but CG increases the residual after the first iteration. **Left:** While the asymptotic convergence rate of CG can be faster than alternating projection, CG does not find a better solution than alternating projection in the first 1000 iterations. **Right:** CG struggles with convergence due to ill-conditioning and does not reach the tolerance δ . In contrast, alternating projection converges. See §4 for more details.

from a modeling perspective (*e.g.*, Hensman et al., 2013, 2015; Titsias, 2009; Snelson and Ghahramani, 2005; Salimbeni et al., 2018; Jankowiak et al., 2020; Katzfuss and Guinness, 2021) and from a numerical methods perspective (*e.g.*, Cutajar et al., 2016; Pleiss et al., 2018; Gardner et al., 2018; Wang et al., 2019; Maddox et al., 2022), and contemporary work even unifies these perspectives to a degree (Artemev et al., 2021; Wenger et al., 2022b). In recent years, numerical methods have increasingly relied on matrix-free iterative methods, which access the kernel matrix through matrix-vector multiplications. These iterations are suitable for GPU acceleration (Gardner et al., 2018) and have shown success on medium to moderately large datasets (Wang et al., 2019), outperforming modeling-based approaches such as stochastic variational GPs (SVGP) (Hensman et al., 2013).

Most GP training and inference approaches based on iterative methods use classic general-purpose al-

gorithms for matrix solves, such as conjugate gradients (CG) (Cutajar et al., 2016; Gardner et al., 2018; Wang et al., 2019), MINRES (Pleiss et al., 2020), or (stochastic) gradient descent (Lin et al., 2023). There is reason to believe that such algorithms are sub-optimal for modern hardware-accelerated Gaussian processes. For example, CG was purpose-built for sparse linear systems that require high-precision solutions. Neither of these properties applies to GP regression: the necessary solves involve dense covariance matrices, and tasks such as hyperparameter optimization can be performed with extremely coarse-grained solves (Wang et al., 2019; Maddox et al., 2022). These characteristics of large-scale dense operations and low precision amenability are in line with existing trends in machine learning (Courbariaux et al., 2015; Micikevicius et al., 2018), but ultimately place Gaussian processes at odds with much of the literature on numerical methods.

Much in the way that deep learning has been revolutionized by purpose-built optimizers that exploit properties of neural networks (Kingma and Ba, 2015; Loshchilov and Hutter, 2019), this paper aims to accelerate GPs with a purpose-built method leveraging (coarse-grained) covariance matrix solves on modern hardware. We introduce an iterative method to compute gradients of the marginal log-likelihood (MLL) and the posterior mean, that improves over CG in the following ways: 1) It requires $\mathcal{O}(n)$ computation per iteration (rather than CG’s $\mathcal{O}(n^2)$); 2) It converges rapidly and monotonically in its early stages (but does not necessarily obtain higher precision than CG); and 3) It demonstrates improved numerical stability in floating point arithmetic.

In summary, we make the following contributions:

- We propose an iterative method to train Gaussian processes, which computes the MLL derivatives and posterior mean via *alternating projection*. Each update accesses only subblocks of the kernel matrix, has linear complexity, and decreases the residual near-monotonically.
- We prove that our algorithm converges linearly at a rate no slower than gradient descent, despite never operating on the full kernel matrix. Empirically, our method achieves a $2\text{-}27\times$ speed-up over CG on a wide range of datasets.
- As a demonstration of its scalability and robustness to ill-conditioning, we are able to train a GP on 4 million data points, the largest dataset reported in the literature to-date without using inducing points or similar modeling approximations—to the best of our knowledge. We find that our method outperforms SVGP by a significant margin at this scale.

2 SETUP AND BACKGROUND

Notation. Let (\mathbf{X}, \mathbf{y}) be a training set of n training inputs $\mathbf{X} = (\mathbf{x}_1 \cdots \mathbf{x}_n)^\top \in \mathcal{X} \subseteq \mathbb{R}^{n \times d}$ and labels $\mathbf{y} = (y_1 \cdots y_n)^\top \in \mathbb{R}^n$. Let the set $\{1, 2, \dots, n\}$ be denoted by $[n]$. Given a matrix $\mathbf{A} \in \mathbb{R}^{n \times n}$ and an index set $I \subseteq [n]$, $\mathbf{A}_I = \mathbf{A}_{I,:}$ is the $|I| \times n$ row-indexed submatrix, $\mathbf{A}_{:,I}$ the $n \times |I|$ column-indexed submatrix, and $\mathbf{A}_{I,I}$ is the $|I| \times |I|$ principal submatrix. We use similar indexing notations for vectors.

Now, let $f : \mathcal{X} \rightarrow \mathbb{R}$ be a latent function, and let $k_\theta : \mathcal{X} \times \mathcal{X} \rightarrow \mathbb{R}$ be a (known) positive definite kernel function with hyperparameters θ . We write $\mathbf{f} = f(\mathbf{X}) = (f(\mathbf{x}_1) \cdots f(\mathbf{x}_n))^\top \in \mathbb{R}^n$. Similarly, $k_\theta(\mathbf{X}, \cdot) : \mathcal{X} \rightarrow \mathbb{R}^n$ denotes the vector-valued function given by $(k(\mathbf{x}_1, \cdot) \cdots k(\mathbf{x}_n, \cdot))^\top \in \mathbb{R}^n$, and $\mathbf{K}_\theta \in \mathbb{R}^{n \times n}$ is the Gram matrix with $[\mathbf{K}_\theta]_{ij} = k_\theta(\mathbf{x}_i, \mathbf{x}_j)$. We omit the subscript θ unless the context needs it.

Gaussian Process Regression. In supervised GP regression, we assume a response-generating function f that is Gaussian process distributed a priori—*i.e.* $f \sim \mathcal{GP}(\mu, k_\theta)$. For simplicity of presentation, we assume without loss of generality an exact observation model—*i.e.* $\mathbf{y} = f(\mathbf{X})$.¹ Given a finite test dataset $\mathbf{x}_1^*, \dots, \mathbf{x}_M^*$, we can obtain a posterior distribution over $f(\mathbf{x}_1^*), \dots, f(\mathbf{x}_M^*)$ using standard Gaussian conditioning rules with the posterior mean and covariance:

$$\begin{aligned} \mathbb{E}[\mathbf{f}^* | \mathbf{f}] &= \boldsymbol{\mu} + \mathbf{K}_{*f} \mathbf{K}^{-1} (\mathbf{y} - \boldsymbol{\mu}), \\ \mathbb{C}[\mathbf{f}^* | \mathbf{f}] &= \mathbf{K}_{**} - \mathbf{K}_{*f} \mathbf{K}^{-1} \mathbf{K}_{f*}. \end{aligned}$$

We refer the reader to Rasmussen and Williams (2006, Ch. 2) for more details.

Hyperparameter Training. The hyperparameters θ of the GP are learned by minimizing the negative marginal log likelihood (MLL) $\ell(\theta) := -\log p(\mathbf{y}; \theta)$. With a Gaussian process prior on f , we have $p(\mathbf{y}; \theta) = \mathcal{N}(\mathbf{y}; \boldsymbol{\mu}, \mathbf{K}_\theta)$, yielding the following minimization:

$$\text{minimize}_\theta \ell(\theta) \stackrel{c}{=} \frac{1}{2} (\mathbf{y}^\top \mathbf{K}_\theta^{-1} \mathbf{y} + \log \det(\mathbf{K}_\theta)) \quad (1)$$

Equation (1) is commonly optimized with first-order methods, which require an (unbiased) estimate of $\frac{\partial \ell(\theta)}{\partial \theta}$. Unfortunately, as (1) cannot be written in the usual $\sum_{i=1}^n \ell(\mathbf{x}_i, y_i)$ form common to many machine learning algorithms, standard minibatching strategies are not readily applicable. Following prior work (*e.g.* Cutajar et al., 2016; Gardner et al., 2018; Wenger et al., 2022a), we use the following unbiased estimate:

$$-\frac{1}{2} \mathbf{y}^\top \mathbf{K}_\theta^{-1} \frac{\partial \mathbf{K}_\theta}{\partial \theta} \mathbf{K}_\theta^{-1} \mathbf{y} + \frac{1}{2l} \sum_{i=1}^l \left(\mathbf{z}_i^\top \mathbf{K}_\theta^{-1} \right) \frac{\partial \mathbf{K}_\theta}{\partial \theta} \mathbf{z}_i, \quad (2)$$

¹Note that we can easily recover an observational noise model by setting $k_\theta(\mathbf{x}, \mathbf{x}') = k_{\text{base}}(\mathbf{x}, \mathbf{x}') + \sigma^2 \mathbb{1}[\mathbf{x} = \mathbf{x}', \mathbf{x} \in \mathbf{X}]$ for some k_{base} and $\sigma > 0$.

where \mathbf{z}_i are i.i.d. random vectors with $\mathbb{E}[\mathbf{z}_i] = \mathbf{0}$ and $\mathbb{E}[\mathbf{z}_i \mathbf{z}_i^\top] = \mathbf{I}$. Note that the first term is an unbiased approximation of $\text{tr}(\mathbf{K}_\theta^{-1} \frac{\partial \mathbf{K}_\theta}{\partial \theta})$. Crucially, computing (2) primarily involves computing solves with \mathbf{K}_θ .

Linear Solves via Iterative Methods. When \mathbf{K} is large, direct methods for solving $\mathbf{K}\mathbf{w} = \mathbf{b}$ are prohibitively slow. Iterative methods, such as conjugate gradients (CG), offer reduced asymptotic complexity (Cutajar et al., 2016), significant GPU acceleration (Gardner et al., 2018), and memory savings if \mathbf{K} is accessed in a map-reduce fashion (Wang et al., 2019; Charlier et al., 2021).

CG minimizes the quadratic objective $\frac{1}{2} \mathbf{w}^\top \mathbf{K} \mathbf{w} - \mathbf{b}^\top \mathbf{w}$ by iteratively searching along conjugated directions. Each iteration requires a $\mathcal{O}(n^2)$ matrix-vector multiplication with \mathbf{K} . In exact arithmetic, CG returns an exact solution after n iterations. In practice for ill-conditioned problems, CG is terminated once the residual $\mathbf{r} = \mathbf{b} - \mathbf{K}\mathbf{w}$ is small enough, e.g., $\|\mathbf{r}\| \leq \delta \|\mathbf{b}\|$ for some predefined tolerance parameter δ .

For GP hyperparameter learning often large values of the tolerance δ are used despite the potential for overfitting (Potapczynski et al., 2021), for example $\delta = 1$ is used in practice (Wang et al., 2019; Maddox et al., 2022) and has been the default setting of CG during training in popular GP software packages (e.g., GPyTorch² and GPflow³).

For hyperparameter training, each MLL derivative evaluation requires a batched linear solve $\mathbf{K}\mathbf{W} = \mathbf{B}$, where $\mathbf{B} = (\mathbf{y} \quad \mathbf{z}_1 \quad \dots \quad \mathbf{z}_l)$ with \mathbf{z}_i are random samples for stochastic MLL derivative estimation in (2).

RKHS. Every kernel $k : \mathcal{X} \times \mathcal{X} \rightarrow \mathbb{R}$ induces a space of functions $\mathcal{H} := \overline{\text{span}}\{k(\mathbf{x}, \cdot) : \mathbf{x} \in \mathcal{X}\} \subset \mathbb{R}^{\mathcal{X}}$, known as a reproducing kernel Hilbert space (RKHS) where the inner product $\langle \cdot, \cdot \rangle_{\mathcal{H}}$ is defined as $\langle k(\mathbf{x}, \cdot), k(\mathbf{x}', \cdot) \rangle_{\mathcal{H}} = k(\mathbf{x}, \mathbf{x}')$ for all $\mathbf{x}, \mathbf{x}' \in \mathcal{X}$.

RKHS Projection. Define the following finite dimensional linear subspaces of \mathcal{H} for indices $I \subseteq [n]$:

$$\begin{aligned} V_{[n]} &= \text{span}\{k(\mathbf{x}_i, \cdot) : i = 1, 2, \dots, n\} \subset \mathcal{H}, \\ V_I &= \text{span}\{k(\mathbf{x}_i, \cdot) : i \in I\} \subseteq V_{[n]}, \end{aligned} \quad (3)$$

By definition these subspaces contain functions of the form $f(\cdot) = \sum_{i=1}^n \alpha_i k(\mathbf{x}_i, \cdot)$ and $f(\cdot) = \sum_{i \in I} \alpha_i k(\mathbf{x}_i, \cdot)$ respectively. We can map any $f \in \mathcal{H}$ onto these subspaces using the projection operator.

Definition 1 (Projection Operator). *Let $V \subseteq \mathcal{H}$ be a closed linear subspace. The projection of any $f \in \mathcal{H}$*

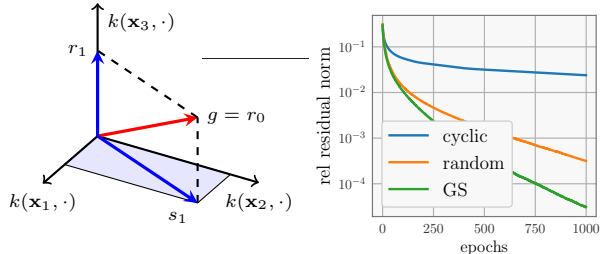


Figure 2: **Left:** Illustration of alternating projection. s_1 is the projection of $g = r_0$ onto the subspace spanned by $k(\mathbf{x}_1, \cdot)$ and $k(\mathbf{x}_2, \cdot)$. The residual $r_1 = g - s_1$ will be projected to other coordinates in the next iteration. **Right:** Gauss-Southwell block selection results in faster convergence than random/cyclic.

onto V is given by the projection operator

$$\text{proj}_V(f) = \underset{g \in V}{\text{argmin}} \quad \frac{1}{2} \|f - g\|_{\mathcal{H}}^2,$$

which is well-defined, i.e. the unique minimizer exists.

Intuitively, the projection operator finds the best approximation of f in V , where approximation error is measured by the norm $\|\cdot\|_{\mathcal{H}}$. For $V = V_{[n]}$ and $V = V_I$, the projection operator has a simple form:

$$\begin{aligned} \text{proj}_{V_{[n]}}(f) &= f(\mathbf{X})^\top \mathbf{K}^{-1} k(\mathbf{X}, \cdot), \\ \text{proj}_{V_I}(f) &= f(\mathbf{X})^\top \mathbf{E}_I^\top \mathbf{K}_{I,I}^{-1} \mathbf{E}_I k(\mathbf{X}, \cdot). \end{aligned} \quad (4)$$

Importantly, these projections only evaluate f and the kernel k on the data \mathbf{X} (or subset \mathbf{X}_I). In other words, it is unnecessary to evaluate f or k outside of \mathbf{X} (or \mathbf{X}_I). The complexity of computing the projection $\text{proj}_V(f)$ depends on the dimension of V : $\text{proj}_{V_{[n]}}(f)$ takes $\mathcal{O}(n^3)$ time and $\text{proj}_{V_I}(f)$ takes $\mathcal{O}(|I|^3)$ time.

3 METHOD

In this section, we develop an iterative method for computing solves $\mathbf{K}^{-1}\mathbf{b}$ by alternating projection. The method supports batch linear solves with multiple right-hand sides, as required by estimating the MLL derivative (2), and is amenable to GPU parallelism. We cast the linear solve as a projection in the RKHS \mathcal{H} and decompose the projection into a sequence of small-scale subproblems. Each subproblem is solved in $\mathcal{O}(n)$ time, allowing frequent updates. Alternating projection typically makes rapid progress in the early stage and finds a medium-precision solution quickly.

High Level Approach. Assume k is strictly positive definite and there is no duplicate data, then there exists $g \in \mathcal{H}$ interpolating \mathbf{b} , i.e. $g(\mathbf{X}) = \mathbf{b}$. The exact

²GPyTorch setting <https://rb.gy/qi8er>

³GPflow setting <https://rb.gy/mozif>

form of g is not important (or unique for that matter); rather, we are interested in its projection onto the subspace $V_{[n]}$, which by (4) is

$$\text{proj}_{V_{[n]}}(g) = \mathbf{b}^\top \mathbf{K}^{-1} k(\mathbf{X}, \cdot),$$

Thus the linear solve can be obtained from the coefficients of the projection $\text{proj}_{V_{[n]}}(g)$.

Directly projecting g onto $V_{[n]}$ is computationally infeasible, as the time complexity is cubic in n . Instead, we partition $[n]$ into subsets $\mathcal{P} = \{I_1, I_2, \dots, I_m\}$. For each subset $I \in \mathcal{P}$, the projection to the linear subspace $V_I \subseteq V_{[n]}$ is cheap, provided that $|I|$ is small. Thus, we construct the (full) projection $\text{proj}_{V_{[n]}}(g)$ by iteratively computing the projection onto the linear subspaces V_I where $I \in \mathcal{P}$.

Starting from $r_0 = g$ and $s_0 = 0$, the j -th iteration selects an index set $I \subseteq [n]$ and updates as follows

$$s_{j+1} = s_j + \text{proj}_{V_I}(r_j) \quad (5)$$

$$r_{j+1} = r_j - \text{proj}_{V_I}(r_j) \quad (6)$$

Intuitively, s_j progressively approximates the true projection $\text{proj}_{V_{[n]}}(g)$, since (5) iteratively adds the projection onto subspaces V_I to the current approximation s_j . Meanwhile, (6) consistently updates the residual. As $j \rightarrow \infty$, s_j converges to the true projection $\mathbf{b}^\top \mathbf{K}^{-1} k(\mathbf{X}, \cdot)$ (Wendland, 2004). See Figure 2 (left panel) for an illustration of alternating projection.

Implicit Representation of $r_j(\cdot)$ Crucially, in the updates (5) and (6), the function r_i is only ever accessed through its evaluation on \mathbf{X} (recall the projection formula (4)). Therefore, we only need to maintain the vector $\mathbf{r}_i = r_i(\mathbf{X}) \in \mathbb{R}^n$ instead of the entire function. The update (6) thus reduces to

$$\begin{aligned} \mathbf{r}_{j+1} &:= \mathbf{r}_j - \text{proj}_{V_I}(r_j)(\mathbf{X}) \\ &= \mathbf{r}_j - \mathbf{K} \mathbf{E}_I^\top \mathbf{K}_{I,I}^{-1} \mathbf{E}_I \mathbf{r}_j \end{aligned} \quad (7)$$

$$= \mathbf{r}_j - \mathbf{K}_{:,I} \mathbf{K}_{I,I}^{-1} [\mathbf{r}_j]_I, \quad (8)$$

where \mathbf{E}_I denotes the rows of the identity matrix corresponding to I . The final line comes from the right multiplication $\mathbf{K} \mathbf{E}_I^\top$ and left multiplication $\mathbf{E}_I \mathbf{r}_j$.

Representing $s_i(\cdot)$ via Kernel Functions. Every s_i is in $V_{[n]}$ and can thus be written as a linear combination $\mathbf{w}_i^\top k(\mathbf{X}, \cdot)$ for some $\mathbf{w}_i \in \mathbb{R}^n$, which is proved by induction. At the 0-th iteration, we see that $s_0(\cdot)$ is the zero function, which can be written as $\mathbf{0}^\top k(\mathbf{X}, \cdot)$. For the j -th iteration, assuming $I \subseteq [n]$ is selected and $s_j = \mathbf{w}_j^\top k(\mathbf{X}, \cdot)$, then we have

$$\begin{aligned} s_{j+1} &= s_j + \text{proj}_{V_I}(r_j) \\ &= \underbrace{\left(\mathbf{w}_j^\top + r_j(\mathbf{X})^\top \mathbf{E}_I^\top \mathbf{K}_{I,I}^{-1} \mathbf{E}_I \right)}_{\mathbf{w}_{j+1}} k(\mathbf{X}, \cdot), \end{aligned}$$

Algorithm 1: Alternating Projection

Input: A batched linear system $\mathbf{K} \mathbf{W} = \mathbf{B}$

Output: The solution $\mathbf{W}^* = \mathbf{K}^{-1} \mathbf{B}$

```

1 Initialize  $\mathbf{W} = \mathbf{O}$  and  $\mathbf{R} = \mathbf{B}$ 
2 for  $t = 1, 2, \dots$  do // epoch
3     for  $j = 1, 2, \dots, m$  do // mini-batch
4         select a block  $I \in \mathcal{P}$  from the partition
5          $\mathbf{W}_I = \mathbf{W}_I + \mathbf{K}_{I,I}^{-1} \mathbf{R}_I$ 
6          $\mathbf{R} = \mathbf{R} - \mathbf{K}_{:,I} \mathbf{K}_{I,I}^{-1} \mathbf{R}_I$ 
7     end
8     if converged then return  $\mathbf{W}$ 
9 end
```

where the last line gives an explicit update on \mathbf{w}_j :

$$\mathbf{w}_{j+1} = \mathbf{w}_j + \mathbf{E}_I^\top \mathbf{K}_{I,I}^{-1} \mathbf{E}_I \mathbf{r}_j. \quad (9)$$

Recall that \mathbf{E}_I simply selects rows/columns. Only entries in \mathbf{w}_j indexed by I need to be updated, while keeping the entries outside I unchanged:

$$\begin{aligned} [\mathbf{w}_{j+1}]_I &= [\mathbf{w}_j]_I + \mathbf{K}_{I,I}^{-1} [\mathbf{r}_j]_I, \\ [\mathbf{w}_{j+1}]_{[n] \setminus I} &= [\mathbf{w}_j]_{[n] \setminus I}. \end{aligned} \quad (10)$$

Summary. (8) and (10) yield an iteration on $s_i(\cdot) = \mathbf{w}_i^\top k(\mathbf{X}, \cdot)$ where the \mathbf{w}_i are obtained through simple matrix operations. Since the s_i are produced by alternating projections, we have $s_i \rightarrow \text{proj}_{V_{[n]}}(g)$ and thus $\mathbf{w}_i \rightarrow \mathbf{K}^{-1} \mathbf{b}$. We summarize this approach in Algorithm 1. Note that the algorithm can be adapted to perform multiple right-hand solves in parallel by replacing $\mathbf{w}_i, \mathbf{r}_i, \mathbf{b}_i$ vectors with matrices $\mathbf{W}, \mathbf{R}, \mathbf{B}$.

Block Selection. Selecting which block to update is crucial for fast convergence. The simplest block selection rules are random selection (sample I uniformly from \mathcal{P}) and cyclic selection ($I = I_j$), which usually converge slowly (see Figure 2). Instead, we select the block I with the largest residual norm

$$I = \underset{I \in \mathcal{P}}{\text{argmax}} \|\mathbf{R}_{I,:}\|_{\mathbb{F}}^2. \quad (11)$$

In the special case that \mathbf{R} is an $n \times 1$ vector, (11) reduces to the Gauss-Southwell (GS) rule (Nutini et al., 2015). (11) is a modification adapted to our setting.

Cached Cholesky. Line 4 requires solving a linear system with the submatrix $\mathbf{K}_{I,I}$. To avoid repeatedly inverting the same matrices, we compute and cache the Cholesky factors of all principal submatrices $\{\mathbf{K}_{I,I} : I \in \mathcal{P}\}$ once whenever the GP hyperparameters are updated (e.g., once per gradient computation). To facilitate parallelism, we partition the blocks evenly so that every block has the same size $|I| = b$ and factorize

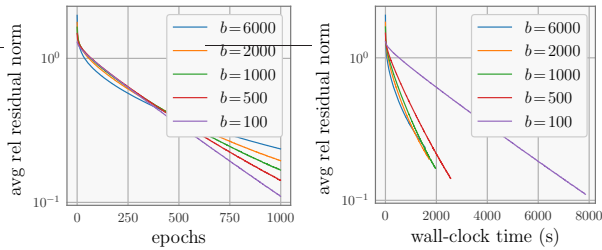


Figure 3: Convergence of alternating projection with different batch sizes b on 3droad. **Left:** Smaller batch sizes converge faster within the same epochs. **Right:** However, smaller batch sizes result in more sequential updates on the GPU and thus longer wall-clock time.

all matrices in a single batch Cholesky call, which takes $\mathcal{O}(nb^2)$ time and $\mathcal{O}(nb)$ memory.

Complexity. The block selection takes $\mathcal{O}(n)$ time. Updating the weights \mathbf{W} takes $\mathcal{O}(b^2)$ time. Updating the residual \mathbf{R} takes $\mathcal{O}(nb)$ time. Each epoch runs $m = n/b$ inner loops and thus takes $\mathcal{O}(nb + n^2)$ time in total. Thus, the complexity of each epoch has the same quadratic complexity as a single CG iteration. A more fine-grained analysis in Appendix F shows that each epoch requires $(2 + \frac{3}{b})n^2 + (2b+1)n$ FLOPs. Thus, for typical batch sizes $1 \ll b \ll n$, each epoch requires roughly $2n^2$ FLOPs, the same number as a single CG iteration. We note that every update in Algorithm 1 has linear (in terms of n) time and memory complexity.

Connection with Coordinate Descent. Interestingly, we can show that Algorithm 1 produces iterates equivalent to coordinate descent on the quadratic form (see §A for details). We will exploit this connection to prove the rate of convergence of Algorithm 1. We introduce this algorithm as alternating projection for two reasons: (a) unlike in coordinate descent, the update rules based on alternating projection maintain the residual \mathbf{R} , which enables efficient block selection strategies like the GS rule without re-evaluating the residual; (b) alternating projection can be easily extended to different settings. For instance, a parallel coordinate descent algorithm was discovered via the connection with (Dykstra’s) alternating projection (Boyle and Dykstra, 1986; Tibshirani, 2017) in the setting of regularized least-squares, which hints that Algorithm 1 may be distributed.

4 CONVERGENCE

Let λ_{\max} and λ_{\min} be the largest and smallest eigenvalues of \mathbf{K} , $\kappa = \lambda_{\max}/\lambda_{\min}$ its condition number, and define $\lambda'_{\max} = \max_{I \in \mathcal{P}} \lambda_{\max}(\mathbf{K}_{I,I})$ as the maximum of the largest eigenvalues of the principal submatrices $\{\mathbf{K}_{I,I} : I \in \mathcal{P}\}$. By leveraging the connection with co-

ordinate descent (Nutini et al., 2022), we can prove an explicit convergence rate for Algorithm 1 when applied to a linear system with multiple right-hand sides.

Theorem 1. *Let \mathbf{W}^* be the (unique) solution of the linear system $\mathbf{K}\mathbf{W} = \mathbf{B}$ and $\mathbf{W}^{(t)}$ its approximation after t epochs of Algorithm 1 using the modified GS rule (11). Then it holds that*

$$\|\mathbf{W}^{(t)} - \mathbf{W}^*\|_{\mathbf{K}}^2 \leq \exp(-t/\kappa') \|\mathbf{W}^{(0)} - \mathbf{W}^*\|_{\mathbf{K}}^2,$$

where $\kappa' = \lambda'_{\max}/\lambda_{\min} \leq \kappa$.

The rate in Theorem 1 improves over gradient descent despite only needing sub matrices, for which the above holds with $\exp(-t/\kappa)$, since generally $\kappa' \leq \kappa$. For comparison, the convergence rate of (batched) CG is $4((\sqrt{\kappa} - 1)/(\sqrt{\kappa} + 1))^{2t} \approx 4 \exp(-4t/\sqrt{\kappa})$ for a sufficiently large condition number $\kappa \gg 1$. The convergence rate of alternating projection is asymptotically faster than that of CG if $\kappa' \leq \frac{1}{4}\sqrt{\kappa}$. In general, we do not expect this condition to hold. However, alternating projection has practical advantages despite a slower asymptotic convergence rate. First, alternating projection performs m times more updates than CG with the same number of FLOPs. Second, alternating projection generally decreases the residual in every epoch, while the CG residual is not monotonic. We empirically observe that CG often increases the residual dramatically in the early stage and it takes time for CG to enter the “linear convergence phase”. In addition, the dependency on κ' suggests that alternating projection implicitly works on better-conditioned matrices, which may imply robustness against ill-conditioning.

Figure 1 shows the above two points in practice. The figure is plotted on two checkpoints at the 50 epoch GP training on the 3droad and house electric datasets respectively. The (batched) linear system $\mathbf{K}^{-1}\mathbf{B}$ has 16 right-hand sides, where $\mathbf{b}_0 = \mathbf{y}$ is the training labels and $\{\mathbf{b}_i\}_{i=1}^{15}$ are *i.i.d.* samples from a Gaussian. We can prove that the random selection strategy in Figure 2 (right panel) achieves a similar rate in Theorem 1, but only in expectation. In practice, the GS rule converges faster than random selection.

The batch size b affects the rate in Theorem 1 through the condition number $\kappa' = \lambda'_{\max}/\lambda_{\min}$. Note that the largest eigenvalue of the principal submatrix is bounded by its trace $\lambda_{\max}(\mathbf{K}_{I,I}) \leq \text{tr}(\mathbf{K}_{I,I})$, where the trace grows linearly in $|I|$. A small batch size $b = |I|$ is likely to have a small λ'_{\max} and a faster convergence rate. We compare the convergence of different batch sizes in Figure 3. Although small batch sizes lead to faster convergence, they generally have a longer running time due to more sequential updates. Therefore, in practice, we recommend using the largest batch

size possible subject to memory constraints. In addition, we note that the convergence rate in Theorem 1 is loose for large batch sizes b . In the extreme case where $b = n$, Algorithm 1 is equivalent to the Cholesky decomposition on the entire matrix \mathbf{K} and thus converges to the exact solution in one update. However, Theorem 1 does not reflect that. The convergence rate in practice may be much faster than the theory predicts.

5 EXPERIMENTS

We evaluate the efficacy of our alternating projections solver in a GP regression task. Our evaluation includes a training dataset of $n = 4M$, which, to the best of our knowledge, is considerably larger than any other dataset where a GP has been applied without inducing points or employing modeling approximations.

All experiments are performed on a single 24 GB NVIDIA RTX A5000 GPUs with single precision floating point, and all numerical algorithms/GP models are implemented in PyTorch/GPyTorch (Gardner et al., 2018). We use the KeOps library (Charlier et al., 2021) to implement all matrix-free numerical algorithms in a map-reduce fashion, thus eliminating the need to store large $n \times n$ kernel matrices in memory.

5.1 Main Result: GP Regression

We first evaluate our method on large-scale GP training tasks. We compare against GPs trained with CG, which is the predominant matrix-free GP training approach (Gardner et al., 2018; Wang et al., 2019; Maddox et al., 2022).

Metrics. Our primary desiderata for GPs are 1) low computational costs for training and 2) generalization. Therefore, we compare the different training methods using the following metrics: 1) the total number of floating point operations (**FLOPs**) normalized by $2n^2$ (the FLOPs of a single matmul), 2) the wall clock **training time**, and 3/4) the trained model’s **RMSE** and **NLL** measured on the test set.

Datasets and Models. We conduct experiments on UCI regression datasets, whose statistics are shown in Table 4. Each dataset is split into 80% training and 20% test. The labels are normalized so that they have zero mean and unit variance. Almost all experiments are averaged over 5 runs. Because of resource constraints, we limit the two largest datasets—House Electric and Gas Sensors—to 3 and 1 run respectively.

We train GP regression models with $\nu = 2.5$ Matérn kernels and a constant prior mean. We optimize the following hyperparameters: a scalar constant for

the prior mean, a d -dimensional kernel lengthscale, a scalar outputscale, and a scalar observational noise parameter σ^2 . We include experiments with $\nu = 1.5$ Matérn kernels in Appendix E.

MLL Optimization. To compute the stochastic MLL gradient (2), we use $l = 15$ random samples \mathbf{z}_i . Thus, all matrix-free methods solve a batched linear system with 16 right-hand sides \mathbf{y} and $\{\mathbf{z}_i\}_{i=1}^{15}$ in each training iteration. On the first five datasets, the GPs are trained by 50 iterations of Adam with a step size 0.1. On house electric and gas sensors, the GPs are trained by 100 iterations of Adam with a step size 0.1.

Alternating Projection Details. As discussed in §4, a large batch size is preferred empirically. We use the largest batch size that we can fit on a 24 GB GPU. The batch sizes b are set as: 6000 on SGEMM, air quality and 3droad; 4000 on song and buzz; 1000 on house electric; 500 on gas sensors. We use the sequential partition \mathcal{P} : the data points from $(j - 1)b + 1$ to jb belong to the j -th block I_j for $j = 1, 2, \dots, n/b$.

The maximum CG iterations and the maximum number of alternating projection epoch is set to 1000. Following GPyTorch’s CG stopping criteria, we terminate the alternating projection solves after (a) the average relative residual norm is strictly smaller than the tolerance $\delta = 1$ or (b) 1000 total epochs, whichever comes first. However, we ensure that at least 11 epochs of alternating projections have been run before termination (again following GPyTorch). We define the average relative residual norm as $\frac{1}{l+1} \sum_{i=0}^l \|\mathbf{r}_i\| / \|\mathbf{b}_i\|$ when there are $l + 1$ right hand sides $(\mathbf{b}_0 \ \mathbf{b}_1 \ \dots \ \mathbf{b}_l)$.

CG Details. We use GPyTorch’s implementation of CG, which uses the same stopping criteria as our alternating projections implementation. Following Wang et al. (2019); Wenger et al. (2022a), we use a pivoted Cholesky preconditioner of size 500 on all datasets except: house electric uses a size 300 and gas sensors uses a size 150 due to GPU memory overflow.

Prediction. At test time, the predictive mean is computed by the same iterative method used for training (e.g., CG for the CG trained GP, alternating projection for the AP trained GP). A limitation of our method is that it does not easily result in a cache for variances. Therefore, we use 1000 Lanczos iterations as in Pleiss et al. (2018); Wang et al. (2019).

Results on $10^5 < n < 10^6$ datasets. Table 4 compares the predictive performance and the training speed of CG-based versus alternating projection-based GPs. Both training procedures produce GPs with similar RMSE and NLL. We conjecture that this similarity occurs because both approaches solve linear systems up to the same tolerance, and thus find similar hyper-

Table 1: Gaussian process training on UCI benchmark datasets. Metrics are computed across multiple runs and reported with \pm one standard deviation.

Dataset	Method	RMSE	NLL	FLOPs/ $2n^2$	Training time	Speed up
SGEMM $n = 241,600$ $d = 14$	CG	0.048 ± 0.000	-1.037 ± 0.001	551 ± 1	$9.1m \pm 0.0$	
	Alt. Proj.	0.046 ± 0.000	-0.999 ± 0.001	550 ± 0	$12.2m \pm 0.2$	0.7 \times
	SVGP	0.086 ± 0.000	-0.934 ± 0.003	NA	$14.8m \pm 0.1$	
air quality $n = 382,168$ $d = 13$	CG	0.261 ± 0.001	0.143 ± 0.004	2965 ± 19	$33.5m \pm 1.5$	
	Alt. Proj.	0.262 ± 0.001	0.137 ± 0.003	550 ± 0	$16.9m \pm 0.5$	2.0 \times
	SVGP	0.363 ± 0.003	0.399 ± 0.006	NA	$23.4m \pm 0.1$	
3droad $n = 434,874$ $d = 3$	CG	0.069 ± 0.000	1.324 ± 0.002	5128 ± 114	$53.2m \pm 2.8$	
	Alt. Proj.	0.076 ± 0.000	1.203 ± 0.001	676 ± 1	$21.1m \pm 0.5$	2.5 \times
	SVGP	0.327 ± 0.002	0.320 ± 0.005	NA	$26.1m \pm 0.1$	
song $n = 515,345$ $d = 90$	CG	0.747 ± 0.002	1.140 ± 0.003	4431 ± 110	$13.8h \pm 0.8$	
	Alt. Proj.	0.749 ± 0.002	1.132 ± 0.002	550 ± 0	$2.7h \pm 0.1$	5.1 \times
	SVGP	0.790 ± 0.002	1.184 ± 0.002	NA	$0.5h \pm 0.0$	
buzz $n = 583,250$ $d = 77$	CG	$0.321^* \pm 0.144$	$0.669^* \pm 1.152$	16726 ± 2724	$31.1h \pm 5.4$	
	Alt. Proj.	0.239 ± 0.001	0.018 ± 0.003	550 ± 0	$2.0h \pm 0.1$	15.6 \times
	SVGP	0.259 ± 0.002	0.066 ± 0.006	NA	$0.6h \pm 0.0$	
house electric $n = 2,049,280$ $d = 11$	CG	-	-	≥ 50441	$\geq 11d$	
	Alt. Proj.	0.030 ± 0.000	-1.148 ± 0.001	1100 ± 0	$9.8h \pm 0.4$	$\geq 26.9\times$
	SVGP	0.050 ± 0.000	-1.549 ± 0.001	NA	$2.1h \pm 0.0$	
gas sensors $n = 4,178,504$ $d = 17$	CG	-	-	-	-	
	Alt. Proj.	0.203	0.070^\dagger	1100	84.5h	
	SVGP	0.330 ± 0.001	0.339 ± 0.003	NA	$8.7h \pm 0.03$	

*: At test time, CG does not reach the tolerance $\delta = 0.01$ after 4000 iterations on some checkpoints.

-: CG does not finish GP training.

†: This predictive variance is calculated using only 500 Lanczos iterations to save time and avoid numerical instability.

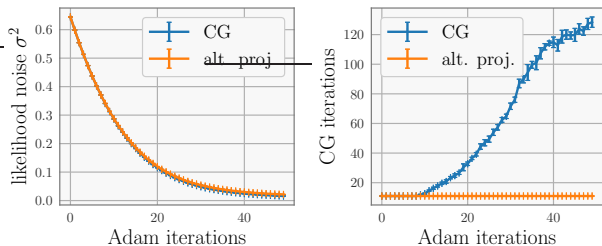


Figure 4: GP training on air quality dataset. **Left:** Because the likelihood noise σ^2 decreases during training, the matrix \mathbf{K} gets more ill-conditioned. **Right:** CG is sensitive to this increased ill-conditioning, while alternating projections is robust.

parameters. One exception is the buzz dataset: CG struggles to converge while training on this dataset, resulting in considerably worse RMSE and NLL.

The primary difference between the two methods is training time. Alternating projection-based training is up to 27 \times faster than CG. The only exception is SGEMM GPU, which seems to be a well-conditioned dataset since CG converges quickly.

For reference, we also report the training/test per-

formance of stochastic variational Gaussian processes (SVGP) (see Appendix E for experimental design details). GPs trained by alternating projection achieve substantially lower RMSE and comparable NLL compared with SVGP. We do note that SVGPs have lower NLL on 3droad and house electric, which we suspect is a limitation of the Lanczos predictive variance estimates used on the alternating projections models. (Note that SVGP’s predictive variances can be computed exactly and do not make use of the Lanczos estimator.) Indeed, in Appendix E we find that the NLL gap shrinks as we increase the rank of the Lanczos variance estimator, suggesting that this gap is not a fundamental limitation of the alternating projections training methodology.

Results on $n \geq 10^6$ datasets. Previous attempts to train GPs using iterative methods on datasets with $n \geq 10^6$ examples have used a large noise constraint $\sigma^2 \geq 0.1$ to improve the conditioning of the kernel matrix (e.g., Wang et al., 2019; Maddox et al., 2022). Since alternating projection is much less conditioning-sensitive than CG (see §5.2), for the first time, we are able to train the model with a much smaller noise constraint $\sigma^2 \geq 10^{-4}$, i.e. the default in GPyTorch for the

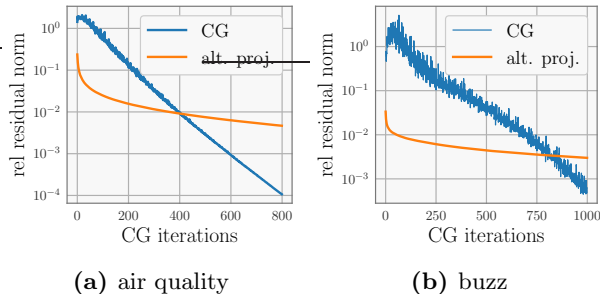


Figure 5: Running CG and alternating projection on test-time solves $\mathbf{K}^{-1}(\mathbf{y} - \boldsymbol{\mu})$. For alternating projection, the x-axis is the number of epochs. **Left:** CG has faster convergence rate, but CG does not reach the test-time tolerance $\delta = 0.01$ much faster. **Right:** Alternating projection reaches the tolerance $\delta = 0.01$ faster despite its slower asymptotic rate.

Gaussian likelihood.⁴ Removing the noise constraint yields much better predictive performance: the RMSE 0.030 is significantly lower than what can be achieved with high-noise constraint models (see Appendix E).

We additionally train a GP on the gas sensors dataset with 4 million data points. To the best of our knowledge, this is the largest dataset trained on using GPs without the use of inducing point or other modeling approximations. CG-based training appears to be intractable on such a large dataset, requiring over a week to train. In contrast, the alternating projections method required 84.5 hours.

5.2 Effect of Kernel Matrix Conditioning

As implied by our theoretical dependence on λ'_{\max} rather than λ_{\max} , we observe that our alternating projections method is less sensitive to ill-conditioning than CG. We demonstrate this phenomenon in Figure 4, which depicts training on the $n \approx 400K$ air quality dataset. Over the course of training, the noise parameter σ^2 decreases for both methods, resulting in an increasingly ill-conditioned kernel matrix (as $\lambda_{\min} \approx \sigma^2$). At the end of training, when $\sigma^2 \approx 0.01$, CG requires over 120 iterations to converge—10 \times as many iterations as the beginning of training. In contrast, alternating projection consistently converges in 11 iterations despite the decreasing noise and increasing condition number. See more datasets in Appendix E.

5.3 Alternating Projection at Test Time

Any linear solver $\mathbf{K}^{-1}\mathbf{b}$ can be used to compute the posterior mean on the test data. We explore alternating projection at test time, as shown in Figure 5

and Table 3 in Appendix E. With a test-time tolerance $\delta = 0.01$, the posterior mean computed by alternating projection is practically the same as CG: the RMSE of both methods are the same up to the 3rd digit after the decimal point. While alternating projection is slightly slower on medium-size datasets such as air quality and 3droad, we observe strong speed up on large datasets such as buzz and house electric. Our method computes the posterior mean 17.2 \times faster in wall-clock time than CG on buzz, and requires only 5 min to compute the posterior mean on house electric.

6 RELATED WORK

The early usage of conjugate gradients in GPs dates back at least to Yang et al. (2004); Shen et al. (2005). They proposed methods speeding up CG by approximate matrix-vector multiplications. More recently, CG has been revisited by Davies (2015); Cutajar et al. (2016). Then, a series of work (Gardner et al., 2018; Wang et al., 2019; Artemev et al., 2021) and software such as GPyTorch (Gardner et al., 2018) and GPflow (Matthews et al., 2017) have popularized CG for GPs.

Alternating projection (Von Neumann, 1949) is a general algorithm finding a point in the intersection of convex sets, enjoying applications in convex optimization (Agmon, 1954) and scattered data approximation (Wendland, 2004). An early work applying coordinate descent with greedy block selection for GP inference is done by Bo and Sminchisescu (2008). However, the algorithm is not parallelizable on modern hardware like GPUs due to the inherent sequential nature of the greedy selection, and lacks an explicit convergence rate with explicit constants. Lin et al. (2023) recently have applied stochastic gradient descent for approximate GP posterior sampling. They also observe CG struggles with convergence in ill-conditioned settings.

7 CONCLUSION

In this work we proposed an alternating projection method with provable linear convergence for solving dense kernel linear systems and applied it to GP training and inference. Our method quickly reaches commonly used tolerances faster than CG, requires only linear time per iteration, and is highly robust to ill-conditioning. Experiments on several large-scale benchmark datasets show that we achieve a 2-27 \times speed-up over CG-based training and a 2-17 \times speed up over CG-based inference with an *increase in predictive performance*. This includes results on datasets as large as 4 million data points which is state-of-the-art for GPs trained with iterative methods without artificially inflating observation noise for stability.

⁴GPyTorch likelihood setting <https://rb.gy/fv41w>

Acknowledgements

JW was supported by the Gatsby Charitable Foundation (GAT3708), the Simons Foundation (542963) and the Kavli Foundation.

References

- Agmon, S. (1954). The relaxation method for linear inequalities. *Canadian Journal of Mathematics*, 6:382–392.
- Artemev, A., Burt, D. R., and van der Wilk, M. (2021). Tighter bounds on the log marginal likelihood of Gaussian process regression using conjugate gradients. In *International Conference on Machine Learning (ICML)*, volume 139, pages 362–372.
- Bertin-Mahieux, T. (2011). YearPredictionMSD. UCI Machine Learning Repository.
- Bo, L. and Sminchisescu, C. (2008). Greedy block coordinate descent for large scale Gaussian process regression. In *Conference on Uncertainty in Artificial Intelligence (UAI)*.
- Boyle, J. P. and Dykstra, R. L. (1986). A method for finding projections onto the intersection of convex sets in Hilbert spaces. In *Advances in Order Restricted Statistical Inference: Proceedings of the Symposium on Order Restricted Statistical Inference*, pages 28–47.
- Charlier, B., Feydy, J., Glaunès, J. A., Collin, F.-D., and Durif, G. (2021). Kernel operations on the GPU, with autodiff, without memory overflows. *Journal of Machine Learning Research*, 22(74):1–6.
- Chen, S. (2019). Beijing Multi-Site Air-Quality Data. UCI Machine Learning Repository.
- Courbariaux, M., Bengio, Y., and David, J.-P. (2015). BinaryConnect: Training deep neural networks with binary weights during propagations. In *Advances in Neural Information Processing Systems (NeurIPS)*, volume 28.
- Cutajar, K., Osborne, M., Cunningham, J., and Filippone, M. (2016). Preconditioning kernel matrices. In *International Conference on Machine Learning (ICML)*, volume 48 of *Proceedings of Machine Learning Research*, pages 2529–2538.
- Davies, A. J. (2015). *Effective implementation of Gaussian process regression for machine learning*. PhD thesis, University of Cambridge.
- Fonollosa, J. (2015). Gas sensor array under dynamic gas mixtures. UCI Machine Learning Repository.
- Gardner, J., Pleiss, G., Weinberger, K. Q., Bindel, D., and Wilson, A. G. (2018). GPyTorch: Black-box matrix-matrix Gaussian process inference with GPU acceleration. In *Advances in Neural Information Processing Systems (NeurIPS)*, volume 31.
- Hebrail, G. and Berard, A. (2012). Individual household electric power consumption. UCI Machine Learning Repository.
- Hensman, J., Fusi, N., and Lawrence, N. D. (2013). Gaussian processes for big data. In *Conference on Uncertainty in Artificial Intelligence (UAI)*.
- Hensman, J., Matthews, A., and Ghahramani, Z. (2015). Scalable variational Gaussian process classification. In *International Conference on Artificial Intelligence and Statistics (AISTATS)*, volume 38, pages 351–360.
- Jankowiak, M., Pleiss, G., and Gardner, J. (2020). Parametric Gaussian process regressors. In *International Conference on Machine Learning (ICML)*, pages 4702–4712.
- Katzfuss, M. and Guinness, J. (2021). A general framework for Vecchia approximations of Gaussian processes. *Statistical Science*, 36(1):124–141.
- Kaul, M. (2013). 3D Road Network (North Jutland, Denmark). UCI Machine Learning Repository.
- Kelly, M., Longjohn, R., and Nottingham, K. (2023). The UCI machine learning repository.
- Kingma, D. and Ba, J. (2015). Adam: A method for stochastic optimization. In *International Conference on Learning Representations (ICLR)*.
- Lin, J. A., Antorán, J., Padhy, S., Janz, D., Hernández-Lobato, J. M., and Terenin, A. (2023). Sampling from Gaussian process posteriors using stochastic gradient descent. In *Advances in Neural Information Processing Systems (NeurIPS)*.
- Loshchilov, I. and Hutter, F. (2019). Decoupled weight decay regularization. In *International Conference on Learning Representations (ICLR)*.
- Maddox, W. J., Potapczynski, A., and Wilson, A. G. (2022). Low-precision arithmetic for fast Gaussian processes. In *Conference on Uncertainty in Artificial Intelligence (UAI)*, volume 180, pages 1306–1316.
- Matthews, A. G. d. G., van der Wilk, M., Nickson, T., Fujii, K., Boukouvalas, A., León-Villagrà, P., Ghahramani, Z., and Hensman, J. (2017). GPflow: A Gaussian process library using TensorFlow. *Journal of Machine Learning Research*, 18(40):1–6.
- Mickevicius, P., Narang, S., Alben, J., Diamos, G., Elsen, E., Garcia, D., Ginsburg, B., Houston, M., Kuchaiev, O., Venkatesh, G., and Wu, H. (2018). Mixed precision training. In *International Conference on Learning Representations (ICLR)*.
- Nutini, J., Laradji, I., and Schmidt, M. (2022). Let’s make block coordinate descent converge faster:

- Faster greedy rules, message-passing, active-set complexity, and superlinear convergence. *Journal of Machine Learning Research*, 23(131):1–74.
- Nutini, J., Schmidt, M., Laradji, I., Friedlander, M., and Koepke, H. (2015). Coordinate descent converges faster with the Gauss-Southwell rule than random selection. In *International Conference on Machine Learning (ICML)*, volume 37, pages 1632–1641.
- Paredes, E. and Ballester-Ripoll, R. (2018). SGEMM GPU kernel performance. UCI Machine Learning Repository.
- Pleiss, G., Gardner, J., Weinberger, K., and Wilson, A. G. (2018). Constant-time predictive distributions for Gaussian processes. In *International Conference on Machine Learning (ICML)*, volume 80, pages 4114–4123.
- Pleiss, G., Jankowiak, M., Eriksson, D., Damle, A., and Gardner, J. (2020). Fast matrix square roots with applications to Gaussian processes and Bayesian optimization. In *Advances in Neural Information Processing Systems (NeurIPS)*, volume 33, pages 22268–22281.
- Potapczynski, A., Wu, L., Biderman, D., Pleiss, G., and Cunningham, J. P. (2021). Bias-free scalable Gaussian processes via randomized truncations. In *International Conference on Machine Learning (ICML)*, volume 139, pages 8609–8619.
- Rasmussen, C. E. and Williams, C. K. (2006). *Gaussian processes for machine learning*. MIT Press.
- Salimbeni, H., Cheng, C.-A., Boots, B., and Deisenroth, M. (2018). Orthogonally decoupled variational Gaussian processes. In *Advances in Neural Information Processing Systems (NeurIPS)*, volume 31.
- Shen, Y., Seeger, M., and Ng, A. (2005). Fast Gaussian process regression using kd-trees. In *Advances in Neural Information Processing Systems (NeurIPS)*, volume 18.
- Snelson, E. and Ghahramani, Z. (2005). Sparse Gaussian processes using pseudo-inputs. In *Advances in Neural Information Processing Systems (NeurIPS)*, volume 18.
- Tibshirani, R. J. (2017). Dykstra's algorithm, admm, and coordinate descent: Connections, insights, and extensions. In *Advances in Neural Information Processing Systems (NeurIPS)*, volume 30.
- Titsias, M. (2009). Variational learning of inducing variables in sparse Gaussian processes. In *International Conference on Artificial Intelligence and Statistics (AISTATS)*, volume 5, pages 567–574.
- Von Neumann, J. (1949). On rings of operators. reduction theory. *Annals of Mathematics*, pages 401–485.
- Wang, K., Pleiss, G., Gardner, J., Tyree, S., Weinberger, K. Q., and Wilson, A. G. (2019). Exact Gaussian processes on a million data points. In *Advances in Neural Information Processing Systems (NeurIPS)*, volume 32.
- Wendland, H. (2004). *Scattered Data Approximation*, volume 17. Cambridge University Press.
- Wenger, J., Pleiss, G., Hennig, P., Cunningham, J., and Gardner, J. (2022a). Preconditioning for scalable Gaussian process hyperparameter optimization. In *International Conference on Machine Learning (ICML)*, volume 162, pages 23751–23780.
- Wenger, J., Pleiss, G., Pförtner, M., Hennig, P., and Cunningham, J. P. (2022b). Posterior and computational uncertainty in Gaussian processes. In *Advances in Neural Information Processing Systems (NeurIPS)*, volume 35, pages 10876–10890.
- Yang, C., Duraiswami, R., and Davis, L. S. (2004). Efficient kernel machines using the improved fast Gauss transform. In *Advances in Neural Information Processing Systems (NeurIPS)*, volume 17.
- Yang, Z., Wilson, A., Smola, A., and Song, L. (2015). A la Carte – Learning Fast Kernels. In *Proceedings of the Eighteenth International Conference on Artificial Intelligence and Statistics*, volume 38, pages 1098–1106.

Large-Scale Gaussian Processes via Alternating Projection: Supplementary Material

A	Connection between Coordinate Descent and Alternating Projection	12
B	Technical Lemmas	13
C	Proof of Theorem 1	14
D	Descriptions of the UCI Datasets in the Experiments	14
E	Additional Experiments	14
E.1	Further Experimental Details	15
E.2	GP Training on House Electric with Large Noise Constraint $\sigma^2 \geq 0.1$	15
E.3	CG Iterations During Training	15
E.4	Increasing Lanczos Iterations Improves NLL	15
E.5	Alternating Projection in Test Time	16
E.6	Training Gaussian Processes with Matérn $\nu = 1.5$	16
F	FLOPs in Algorithm 1	17

A Connection between Coordinate Descent and Alternating Projection

This section shows the connection between Algorithm 1 and coordinate descent, as shown in Algorithm 2.

Algorithm 2: Block Coordinate Descent

Input: A kernel linear system $\mathbf{KW} = \mathbf{B}$
Output: The solution $\mathbf{K}^{-1}\mathbf{B}$

```

1 Initialize  $\mathbf{W} = \mathbf{O}$ 
2 for  $i = 1, 2, \dots$  do // epoch
3   for  $j = 1, 2, \dots, m$  do // mini-batch
4     select a block  $I \in \{I_1, I_2, \dots, I_m\}$ 
5      $\mathbf{W}_I = \mathbf{K}_{I,I}^{-1}(\mathbf{B}_I - \mathbf{K}_{I,-I}\mathbf{W}_{-I})$ 
6   end
7   if converged then
8     return  $\mathbf{W}$ 
9 end
```

Observe that the minimizer of the quadratic objective

$$h(\mathbf{W}) = \frac{1}{2}\text{tr}(\mathbf{W}^\top \mathbf{K} \mathbf{W}) - \text{tr}(\mathbf{B}^\top \mathbf{W}) \quad (12)$$

is exactly the solution $\mathbf{K}^{-1}\mathbf{B}$ of the linear system $\mathbf{KW} = \mathbf{B}$.

Given a partition of indices $\{I_1, I_2, \dots, I_m\}$ where $I_i \cap I_j = \emptyset$ for all $i \neq j$ and $\cup_{i=1}^m I_i = [n]$, coordinate descent minimizes (12) by minimizing over a subset of variables \mathbf{W}_{I_i} in each iteration. The derivative of (12) is

$$\nabla h(\mathbf{W}) = \mathbf{KW} - \mathbf{B}.$$

Thus, the derivative w.r.t. the subblock \mathbf{W}_{I_i} is

$$\begin{aligned} [\nabla h(\mathbf{W})]_{I_i} &= \mathbf{K}_{I_i} \mathbf{W} - \mathbf{B}_{I_i} \\ &= (\mathbf{K}_{I_i, I_i} \quad \mathbf{K}_{I_i, -I_i}) \begin{pmatrix} \mathbf{W}_{I_i} \\ \mathbf{W}_{-I_i} \end{pmatrix} - \mathbf{B}_{I_i} \end{aligned}$$

where the second line splits \mathbf{K}_{I_i} and \mathbf{W} into two blocks. The index $-I_i = [n] \setminus I_i$ denotes the complement of I_i . Setting the derivative to zero gives the following update

$$\mathbf{W}_{I_i}^{(j+1)} = \mathbf{K}_{I_i, I_i}^{-1}(\mathbf{B}_{I_i} - \mathbf{K}_{I_i, -I_i} \mathbf{W}_{-I_i}^{(j)})$$

which minimizes (12) over \mathbf{W}_{I_i} exactly. The full algorithm of coordinate descent is shown in Algorithm 2.

The following lemma shows the \mathbf{R} matrix in Algorithm 1 is indeed the residual of the linear system. This lemma will be useful in proving the equivalence between Algorithm 1 and Algorithm 2.

Lemma 1. *Let $\mathbf{R}^{(j)}$ and $\mathbf{W}^{(j)}$ be the residual and weight after j updates of Algorithm 1. Then we have*

$$\mathbf{R}^{(j)} = \mathbf{B} - \mathbf{KW}^{(j)}.$$

Proof. The proof is an induction on the number of updates j . At the initialization $j = 0$, the equality holds trivially. Suppose after the j -th update we have $\mathbf{R}^{(j)} = \mathbf{B} - \mathbf{KW}^{(j)}$. All we need to do is to verify this equality in the case of $j + 1$ by direct calculation:

$$\begin{aligned} \mathbf{B} - \mathbf{KW}^{(j+1)} &= \mathbf{B} - \mathbf{K}(\mathbf{W}^{(j)} + \mathbf{E}_I^\top \mathbf{K}_{I,I}^{-1} \mathbf{E}_I \mathbf{R}^{(j)}) \\ &= \mathbf{R}^{(j)} - \mathbf{K} \mathbf{E}_I^\top \mathbf{K}_{I,I}^{-1} \mathbf{E}_I \mathbf{R}^{(j)} \\ &= \mathbf{R}^{(j+1)} \end{aligned}$$

where the first line uses the update rule (7) of $\mathbf{W}^{(j)}$ and the last line uses the update rule (9) of $\mathbf{R}^{(j)}$. \square

With Lemma 1, now we can show the equivalence between Algorithm 1 and Algorithm 2.

Lemma 2. *Let $\mathbf{W}^{(j)}$ be the weight produced by Algorithm 1 after j updates. Then, we have*

$$\begin{aligned}\mathbf{W}_I^{(j+1)} &= \mathbf{K}_{I,I}^{-1}(\mathbf{B}_I - \mathbf{K}_{I,-I}\mathbf{W}_{-I}^{(j)}) \\ \mathbf{W}_{-I}^{(j+1)} &= \mathbf{W}_{-I}^{(j)}\end{aligned}$$

where $-I = [n] \setminus I$. Thus, Algorithm 1 produces the same iterates as Algorithm 2.

Proof. Recalling the update rule (9), we have

$$\mathbf{W}^{(j+1)} = \mathbf{W}^{(j)} + \mathbf{E}_I^\top \mathbf{K}_{I,I}^{-1} \mathbf{E}_I \mathbf{R}^{(j)}.$$

Thanks to \mathbf{E}_I^\top , entries outside I are unchanged and thus $\mathbf{W}_{-I}^{(j+1)} = \mathbf{W}_{-I}^{(j)}$. It remains to verify the entries indexed by I . By Lemma 1, we can plug in $\mathbf{R}^{(j)} = \mathbf{B} - \mathbf{K}\mathbf{W}^{(j)}$ and thus

$$\begin{aligned}\mathbf{W}_I^{(j+1)} &= \mathbf{W}_I^{(j)} + \mathbf{K}_{I,I}^{-1} \mathbf{E}_I (\mathbf{B} - \mathbf{K}\mathbf{W}^{(j)}) \\ &= \mathbf{W}_I^{(j)} + \mathbf{K}_{I,I}^{-1} (\mathbf{B}_I - \mathbf{K}_I \mathbf{W}^{(j)}) \\ &= \mathbf{W}_I^{(j)} + \mathbf{K}_{I,I}^{-1} (\mathbf{B}_I - \mathbf{K}_{I,I} \mathbf{W}_I^{(j)} - \mathbf{K}_{I,-I} \mathbf{W}_{-I}^{(j)}) \\ &= \mathbf{K}_{I,I}^{-1} (\mathbf{B}_I - \mathbf{K}_{I,-I} \mathbf{W}_{-I}^{(j)})\end{aligned}$$

where the second line uses the definition of \mathbf{E}_I ; the third line split the matrix \mathbf{K}_I into blocks $\mathbf{K}_I = (\mathbf{K}_{I,I} \quad \mathbf{K}_{I,-I})$; the last line is straightforward algebra. \square

B Technical Lemmas

Lemma 3. *The quadratic objective function (12) satisfies the Polyak-Lojasiewicz (PL) inequality*

$$\frac{1}{2} \|\nabla h(\mathbf{W})\|_{\mathbb{F}}^2 \geq \lambda_{\min}(h(\mathbf{W}) - h(\mathbf{W}^*)).$$

Proof. If \mathbf{W} has only a single column this follows directly from the strong convexity of the quadratic function. When \mathbf{W} has multiple columns, h is a separable function across each column. Therefore, h is also λ_{\min} strongly convex which implies the PL inequality. \square

Lemma 4. *For $h(\mathbf{W})$ as in (12), it holds that*

$$h(\mathbf{W}) - h(\mathbf{W}^*) = \frac{1}{2} \|\mathbf{W} - \mathbf{W}^*\|_{\mathbf{K}}^2.$$

Proof. Using $\mathbf{B} = \mathbf{K}\mathbf{W}^*$, we have

$$\begin{aligned}h(\mathbf{W}) - h(\mathbf{W}^*) &= \frac{1}{2} \langle \mathbf{W}, \mathbf{K}\mathbf{W} \rangle - \langle \mathbf{B}, \mathbf{W} \rangle - \frac{1}{2} \langle \mathbf{W}^*, \mathbf{K}\mathbf{W}^* \rangle + \langle \mathbf{B}, \mathbf{W}^* \rangle \\ &= \frac{1}{2} \langle \mathbf{W}, \mathbf{K}\mathbf{W} \rangle - \langle \mathbf{K}\mathbf{W}^*, \mathbf{W} \rangle - \frac{1}{2} \langle \mathbf{W}^*, \mathbf{K}\mathbf{W}^* \rangle + \langle \mathbf{K}\mathbf{W}^*, \mathbf{W}^* \rangle \\ &= \frac{1}{2} \langle \mathbf{W}, \mathbf{K}\mathbf{W} \rangle - \langle \mathbf{K}\mathbf{W}^*, \mathbf{W} \rangle + \frac{1}{2} \langle \mathbf{W}^*, \mathbf{K}\mathbf{W}^* \rangle \\ &= \frac{1}{2} \|\mathbf{W} - \mathbf{W}^*\|_{\mathbf{K}}^2.\end{aligned}$$

\square

C Proof of Theorem 1

Theorem 1. *Let \mathbf{W}^* be the (unique) solution of the linear system $\mathbf{K}\mathbf{W} = \mathbf{B}$ and $\mathbf{W}^{(t)}$ its approximation after t epochs of Algorithm 1 using the modified GS rule (11). Then it holds that*

$$\|\mathbf{W}^{(t)} - \mathbf{W}^*\|_{\mathbf{K}}^2 \leq \exp(-t/\kappa') \|\mathbf{W}^{(0)} - \mathbf{W}^*\|_{\mathbf{K}}^2,$$

where $\kappa' = \lambda'_{\max}/\lambda_{\min} \leq \kappa$.

Proof. For any residual \mathbf{R} , note the following inequality

$$\|\mathbf{R}\|_{\mathbb{F}}^2 = \sum_{I \in \mathcal{P}} \|\mathbf{R}_{I,:}\|_{\mathbb{F}}^2 \leq |\mathcal{P}| \cdot \max_{I \in \mathcal{P}} \|\mathbf{R}_{I,:}\|_{\mathbb{F}}^2 = m \cdot \max_{I \in \mathcal{P}} \|\mathbf{R}_{I,:}\|_{\mathbb{F}}^2. \quad (13)$$

The improvement on the objective h as in (12) after the update in the j -th iteration is bounded by

$$\begin{aligned} h(\mathbf{W}^{(j+1)}) - h(\mathbf{W}^{(j)}) &= -\frac{1}{2} \|\mathbf{R}_{I,:}^{(j)}\|_{\mathbf{K}_{I,I}^{-1}}^2 \\ &\leq -\frac{1}{2\lambda'_{\max}} \|\mathbf{R}_{I,:}^{(j)}\|_{\mathbb{F}}^2 \\ &\leq -\frac{1}{2m\lambda'_{\max}} \|\mathbf{R}^{(j)}\|_{\mathbb{F}}^2 \end{aligned}$$

where the last inequality is due to the Gauss-Southwell selection rule and (13). Subtract $h^* = h(\mathbf{W}^*)$ from both sides. Then, we have

$$\begin{aligned} h(\mathbf{W}^{(j+1)}) - h^* &= h(\mathbf{W}^{(j)}) - h^* - \frac{1}{2m\lambda'_{\max}} \|\mathbf{R}^{(j)}\|_{\mathbb{F}}^2 \\ &\leq \left(1 - \frac{\lambda_{\min}}{m\lambda'_{\max}}\right) (h(\mathbf{W}^{(j)}) - h^*) \\ &\leq \left(1 - \frac{1}{m\kappa'}\right) (h(\mathbf{W}^{(j)}) - h^*) \end{aligned}$$

where the second line uses $\mathbf{R}^{(j)} = \mathbf{B} - \mathbf{K}\mathbf{W}^{(j)} = -\nabla h(\mathbf{W}^{(j)})$ by Lemma 1 and the PL inequality by Lemma 3. Using the inequality $(1-x)^t \leq \exp(-tx)$, we obtain a convergence rate in the number of updates j

$$h(\mathbf{W}^{(j+1)}) - h^* \leq \exp\left(-\frac{j}{m\kappa'}\right) (h(\mathbf{W}^{(0)}) - h^*).$$

Since each epoch has m updates, the convergence rate in the number of epochs t is

$$h(\mathbf{W}^{(t+1)}) - h^* \leq \exp\left(-\frac{t}{\kappa'}\right) (h(\mathbf{W}^{(0)}) - h^*).$$

By Lemma 4, the left and right hand sides can be written as $\|\mathbf{W}^{(t)} - \mathbf{W}^*\|_{\mathbf{K}}^2$ and $\|\mathbf{W}^{(0)} - \mathbf{W}^*\|_{\mathbf{K}}^2$ respectively, which concludes the proof. \square

D Descriptions of the UCI Datasets in the Experiments

This section lists the relevant information of the datasets with citations. The datasets used in the papers are SGEMM GPU (Paredes and Ballester-Ripoll, 2018), air quality (Chen, 2019), 3droad (Kaul, 2013), song (Bertin-Mahieux, 2011), buzz (Yang et al., 2015), house electric (Hebrail and Berard, 2012), and gas sensors (Fonollosa, 2015). All of them are downloaded from the UCI machine learning repository (Kelly et al., 2023).

E Additional Experiments

This section presents more experimental details and additional experiments.

E.1 Further Experimental Details

GP Training. All Gaussian processes, including the stochastic variational Gaussian processes, use an observation noise constraint $\sigma^2 \geq 10^{-4}$, which is the default in GPyTorch. For the stochastic trace estimation (2), we use $\ell = 15$ random probe vectors. For CG, the probe vectors are sampled from $\mathcal{N}(\mathbf{0}, \mathbf{P})$, where \mathbf{P} is the pivoted Cholesky preconditioner. Again, these settings are the default in GPyTorch. For alternating projection, the probe vectors are sampled from the Rademacher distribution.

Preconditioning. CG uses the pivoted Cholesky preconditioner both in training and test. During training, the preconditioner size is 500 on SGEMM, air quality, 3droad, song and buzz; 300 on house electric; 150 on gas sensors. We decrease the preconditioner size on house electric and gas sensors due to GPU memory overflow. During test, the preconditioner size is 500 on SGEMM, air quality, 3droad, song, buzz and house electric; 300 on gas sensors. Again, we decrease the preconditioner size on gas sensors due to GPU memory flow.

SVGP Training. All SVGPs use 1024 inducing points and a batch size of 4096. On the first six datasets, SVGPs are trained with 50 iterations of Adam with a step size 0.01 and another 150 iterations of Adam with a step size 0.001. On gas sensors, we train the SVGP with 50 iterations of Adam with a step size 0.01 followed by 350 iterations of Adam with a step size 0.001.

The right panel of Figure 2 is produced on with an alternating projection-trained GP on air quality with batch size 1000. The linear system solved in the figure is $\mathbf{K}^{-1}\mathbf{y}$.

Figure 3 is plotted with an alternating projection-trained GP on 3droad. The linear system in the figure is $\mathbf{K}^{-1}(\mathbf{y} \quad \mathbf{z}_1 \quad \mathbf{z}_2 \quad \cdots \quad \mathbf{z}_{15})$ where \mathbf{z}_i are sampled from a standard Gaussian distribution.

E.2 GP Training on House Electric with Large Noise Constraint $\sigma^2 \geq 0.1$

We compare Gaussian processes on house electric trained with two different noise constraints $\sigma^2 \geq 0.1$ and $\sigma^2 \geq 10^{-4}$, as shown Table 2. We observe significant improvements on both RMSE and NLL when the noise is smaller. In particular, the GP trained with small noise constraint $\sigma^2 \geq 10^{-4}$ has 40% smaller RMSE and significantly smaller NLL. This indicates that artificially inflating the observation noise σ^2 , while making the kernel matrix well-conditioned, ultimately hurts the predictive performance.

With alternating projection, training the GP with small noise constraint $\sigma^2 \geq 10^{-4}$ is as fast as the GP with large noise constraint $\sigma^2 \geq 10^{-1}$.

Table 2: Comparison of GP training on the house electric dataset with large noise constraint $\sigma^2 \geq 0.1$ and small noise constraint $\sigma^2 \geq 10^{-4}$.

Dataset	Method	RMSE	NLL	FLOPs / $2n^2$	Time
house electric	CG ($\sigma^2 \geq 10^{-1}$)	0.050 ± 0.000	-0.196 ± 0.000	1200 ± 8	$9.6\text{h} \pm 0.6$
$n = 2,049,280$	Alt. Proj. ($\sigma^2 \geq 10^{-1}$)	0.053 ± 0.000	-0.197 ± 0.000	1100 ± 0	$9.8\text{h} \pm 0.4$
$d = 11$	Alt. Proj. ($\sigma^2 \geq 10^{-4}$)	0.030 ± 0.000	-1.148 ± 0.001	1100 ± 0	$9.8\text{h} \pm 0.4$

E.3 CG Iterations During Training

Figure 4 in the main paper is produced on air quality. This section presents figures on more datasets, as shown in Figure 6. We observe similar phenomenon: as the noise decreases during training, the number of CG iteration increases; in contrast, alternating projection converges steadily.

E.4 Increasing Lanczos Iterations Improves NLL

In the experiment, we use 1000 Lanczos iterations to compute the predictive variance and the test negative log likelihood (NLL). This section investigates the relation between test NLL and the Lanczos iterations, as shown in Figure 7. We empirically observe that increasing the Lanczos iterations always decreases the test NLL. This suggests that the true NLL of the GPs may be even lower than what is reported in Table 4.

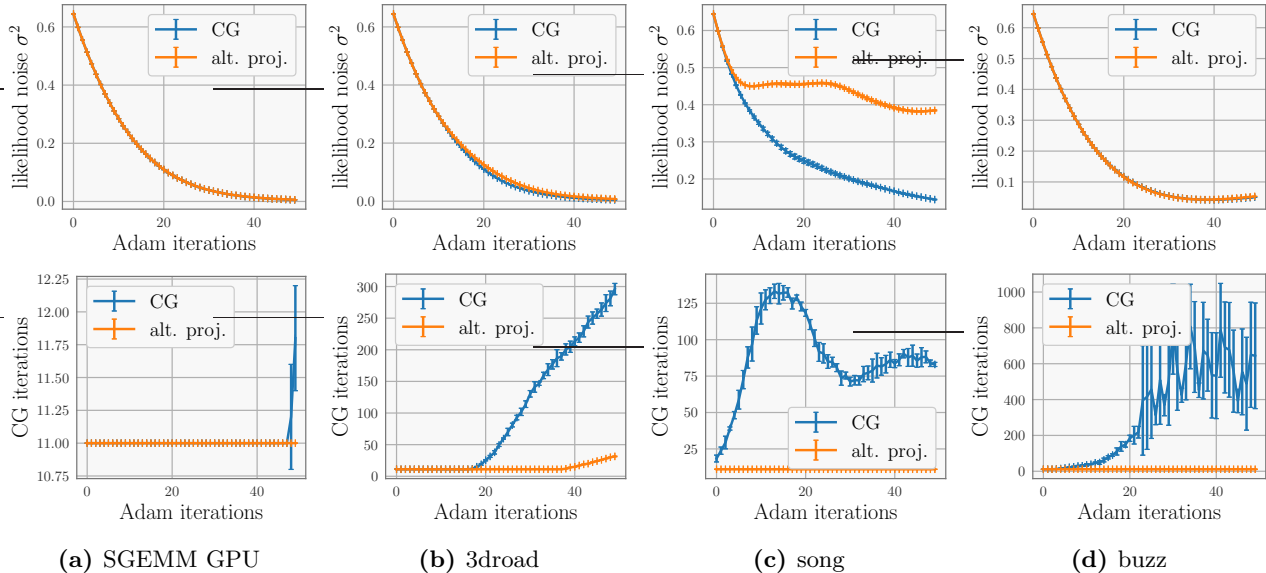


Figure 6: The observation noise σ^2 and the number of CG iterations/alternating projection epochs during training. **Top:** The observation noise σ^2 decreases as the training goes. **Bottom:** CG takes more iterations to converge as the observation noise decreases during training. However, alternating projection is less sensitive to the decrease of observation noise.

E.5 Alternating Projection in Test Time

This section compares alternating projection and CG in the test time. We use CG and alternating projection to compute the predictive mean and the RMSE of alternating projection-trained GPs, as shown Table 3. CG and alternating projection report virtually the same RMSE (exactly the same up to the third digit after the decimal point). However, we observe significant speed up on large datasets. On the four largest datasets, alternating projection achieves $2.3\times$ to $72.3\times$ speed up. In particular, the predictive mean on house electric can be computed in 5 min with alternating projection.

Table 3: Compute the predictive mean and the RMSE of the GPs using CG and alternating projection.

Dataset	RMSE		Time		Speed up
	CG	Alt. Proj.	CG	Alt. Proj.	
SGEMM	0.046 ± 0.000	0.046 ± 0.000	35.0s ± 1.1	13.5s ± 0.3	0.4 \times
air quality	0.256 ± 0.001	0.256 ± 0.001	2.8s ± 0.3	3.6s ± 0.8	0.7 \times
3droad	0.076 ± 0.000	0.076 ± 0.000	5.8m ± 0.4	9.6m ± 0.6	0.6 \times
song	0.749 ± 0.002	0.749 ± 0.001	38.1m ± 0.7	16.4m ± 1.0	2.3 \times
buzz	0.240 ± 0.001	0.239 ± 0.001	1.2h ± 0.6	4.4m ± 1.2	17.2 \times
house electric	0.032 ± 0.000	0.030 ± 0.000	5.6h ± 0.6	4.7m ± 0.2	72.3 \times
gas sensors	0.203	0.203	16.1h	27.7m	34.9 \times

E.6 Training Gaussian Processes with Matérn $\nu = 1.5$

Lastly, we report results using Matérn $\nu = 1.5$. The experimental settings are exactly the same as Matérn $\nu = 2.5$ GPs. We observe similar phenomenon: while CG-trained GPs and alternating projection-trained GPs have similar RMSE and NLL, alternating projection achieves $1.4\times$ to $27.2\times$ speed up against CG.

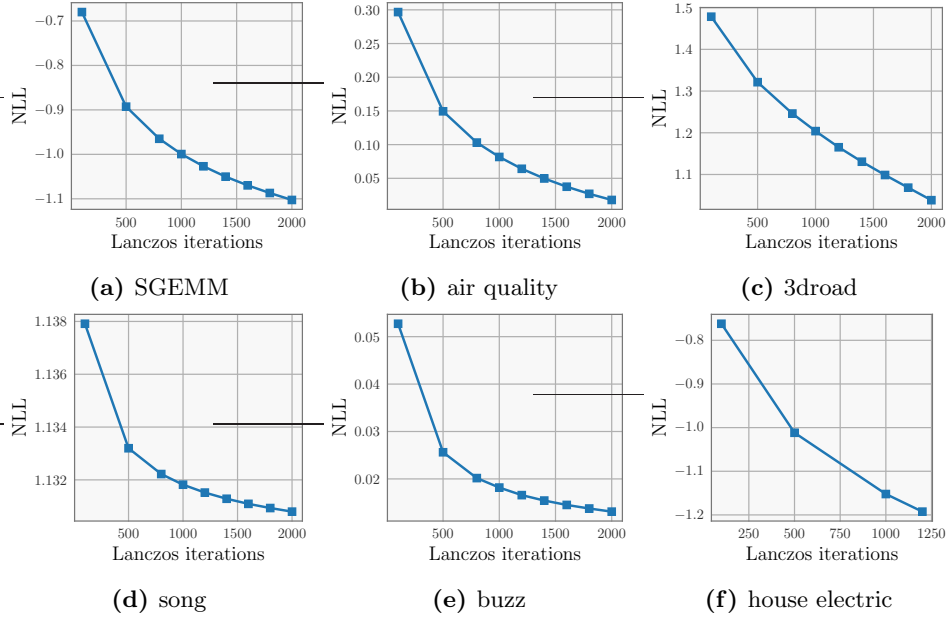


Figure 7: Test negative log likelihood (NLL) *vs.* the number of Lanczos iterations. Empirically, the test NLL decreases as the number of Lanczos iterations increases on all datasets.

F FLOPs in Algorithm 1

The following table gives floating point operations (FLOPs) and memory complexity of Algorithm 1. There is no hidden constant in the leading term. Throughout, we assume $l \ll n$ and $1 \ll b \ll n$.

Table 4: Gaussian process training on UCI benchmark datasets with Matérn $\nu = 1.5$. Metrics are computed across multiple runs and reported with \pm one standard deviation.

Dataset	Method	RMSE	NLL	FLOPs/ $2n^2$	Training time	Speed up
SGEMM $n = 241,600$ $d = 14$	CG	0.048 \pm 0.000	-1.071 \pm 0.001	550 \pm 0	8.9m \pm 0.2	
	Alt. Proj.	0.048 \pm 0.000	-1.060 \pm 0.001	550 \pm 0	12.1m \pm 0.2	0.7 \times
	SVGP	0.085 \pm 0.000	-0.932 \pm 0.001	NA	18.3m \pm 0.1	
air quality $n = 382,168$ $d = 13$	CG	0.227 \pm 0.002	0.131 \pm 0.003	1825 \pm 26	22.5m \pm 1.2	
	Alt. Proj.	0.253 \pm 0.001	0.033 \pm 0.002	550 \pm 0	16.1m \pm 0.5	1.4 \times
	SVGP	0.358 \pm 0.002	0.387 \pm 0.005	NA	28.8m \pm 0.1	
3droad $n = 434,874$ $d = 3$	CG	0.065 \pm 0.001	1.062 \pm 0.003	6086 \pm 142	44.4m \pm 2.2	
	Alt. Proj.	0.069 \pm 0.001	0.896 \pm 0.002	572 \pm 1	16.5m \pm 0.3	2.7 \times
	SVGP	0.319 \pm 0.002	0.294 \pm 0.007	NA	32.4m \pm 0.1	
song $n = 515,345$ $d = 90$	CG	0.743 \pm 0.001	1.135 \pm 0.003	4393 \pm 159	13.7h \pm 0.6	
	Alt. Proj.	0.746 \pm 0.002	1.129 \pm 0.002	550 \pm 0	2.6h \pm 0.0	5.3 \times
	SVGP	0.790 \pm 0.002	1.184 \pm 0.002	NA	0.6h \pm 0.0	
buzz $n = 583,250$ $d = 77$	CG	0.238 \pm 0.000	0.027 \pm 0.002	13608 \pm 2299	25.4h \pm 4.7	
	Alt. Proj.	0.238 \pm 0.001	0.002 \pm 0.004	550 \pm 0	1.9h \pm 0.1	13.4 \times
	SVGP	0.255 \pm 0.002	0.049 \pm 0.009	NA	0.7h \pm 0.0	
house electric $n = 2,049,280$ $d = 11$	CG	-	-	-	\geq 11d	
	Alt. Proj.	0.029 \pm 0.000	-1.321 \pm 0.000	1100 \pm 0	9.7h \pm 0.1	\geq 27.2 \times
	SVGP	0.048 \pm 0.000	-1.580 \pm 0.003	NA	2.6h \pm 0.0	
gas sensors $n = 4,178,504$ $d = 17$	CG	-	-	-	-	
	Alt. Proj.	0.201	0.245[†]	1100	42h*	
	SVGP	0.311 \pm 0.002	0.286 \pm 0.004	NA	10.6h \pm 0.1	

[†]: This predictive variance is calculated using only 500 Lanczos iterations to save time and avoid numerical instability.

*: Time measured on a A100 GPU.

Table 5: FLOPs Counting in Algorithm 1.

Operation	FLOPs	Memory
Cache Cholesky decomposition of $\{\mathbf{K}_{I,I} : I \in \mathcal{P}\}$	$\frac{1}{3}nb^2$	nb
GS rule $I = \operatorname{argmax}_{I \in \mathcal{P}} \ \mathbf{R}_{I,:}\ _{\mathbb{F}}^2$	$2nl$	-
$\mathbf{W}_I = \mathbf{W}_I + \mathbf{K}_{I,I}^{-1}\mathbf{R}_I$	$(b^2 + b)l$	-
$\mathbf{R} = \mathbf{R} - \mathbf{K}_{:,I}\mathbf{K}_{I,I}^{-1}\mathbf{R}_I$	$(b^2 + 2nb + n)l$	nb
total FLOPs of a single epoch	$((2 + \frac{3}{b})n^2 + (2b + 1)n)l$	$2nb$